Weak-Antilocalization signatures in the magnetotransport properties of individual electrodeposited Bi Nanowires

1 February 2010

N Marcano[1,2], S Sangiao[1,2,3], M Plaza[4], L Pérez[4], A Fernández Pacheco[1,2,3], R Córdoba[2,3], M C Sánchez[4], L Morellón[1,2,3], M R Ibarra[1,2,3] and J M De Teresa[1,2]

[1]Instituto de Ciencia de Materiales de Aragón, Universidad de Zaragoza-CSIC, Zaragoza, 50009, Spain

[2] Departamento de Física de la Materia Condensada, Universidad de Zaragoza, 50009, Spain

[3]Instituto de Nanociencia de Aragón, Universidad de Zaragoza, Zaragoza, 50009, Spain

[4]Departamento de Física de Materiales, Universidad Complutense de Madrid, Madrid, Spain

Abstract

We study the electrical resistivity of individual Bi nanowires of diameter 100 nm fabricated by electrodeposition using a four-probe method in the temperature range 5- 300 K with magnetic fields up to 90 kOe. Low-resistance ohmic contacts to individual Bi nanowires are achieved using a focused ion beam to deposit W-based nanocontacts. Magnetoresistance measurements show evidence for weak antilocalization at temperatures below 10 K, with a phase-breaking length of 100 nm.

PACS: 73.20.Fz, 73.63.Nm, 81.15 Jj, 75.47.Jn

*corresponding author: marcanon@unizar.es

During the last years, there has been a great interest in *Bi Nanowires (NWs)* since they provide an attractive scenario for fundamental investigation of both classical and quantum finite-size effects, due to the unusual electronic structure of Bi. They are of special interest for thermoelectric applications due to the unique properties of bulk Bi, such as its small electron effective mass, the high anisotropy of its Fermi surface and the low thermal conductivity [1]. In particular, the small Bi electron effective mass ($\sim 0.001m_e$) has motivated an active investigation of quasi-one dimensional phenomena such as the wire-boundary scattering effect and quantum confinement effects on the electronic transport properties of quasi 1D-systems [2,3].

Localization effects caused by quantum interference effects in disordered systems with reduced dimensionality have been studied over the past two decades [4]. In the case of systems with large spin-orbit interaction, such as Bi, they are referred to as *weak antilocalization (WAL)* effects and manifest as a positive correction to the conductance of the system [5-7]. In a system with a diffusion constant D, the relevant scale for coherence in phase is $L_\varphi = (D\tau_\varphi)^{1/2}$ (τ_φ is the phase-breaking time of the electron wave function) which determines the effective dimensionality of a system with respect to WAL effects. Thus, for a wire with a small diameter (*W*) so that $L_\varphi > W$, the localization behaviour should be regarded as one dimensional. In the case of Bi, the signature from WAL effects can be overshadowed by the contribution coming from the classical or ordinary *magnetoresistance (MR)* caused by the curving of the electron trajectory by the magnetic field (Lorentz force). The magnitude of the latter, which is proportional to $(\omega_c\tau)^2$ where ω_c is the cyclotron frequency and τ is the relaxation time, is much larger than in metals since the characteristic term $\omega_c\tau$ is much larger in Bi due to the low effective mass and large relaxation time. In particular, Bi NW arrays show ordinary MR values of several 100's at 50 kOe at low temperature [8] which is typically 2-3 orders of magnitude larger than the contribution due to WAL [9]. This fact limited the observation of signatures of localization effects to very low temperatures (< 4 K) and low magnetic fields which did not allow a quantitative analysis of localization effects.

However, WAL effects can be enhanced with the reduction of dimensionality since the classical MR is expected to drop significantly. NWs represent an excellent playground for the investigation of 1D WAL effects.

To date, however, most of the reported studies on Bi-NWs focused on electronic transport properties in polycrystalline or single-crystal Bi arrays of NW using two-probe technique. The main reason for the lack of four-probe measurements on individual NW is the difficulty in making good electrical ohmic contacts due to a native 10 nm thick Bi oxide coating that forms on the surface of the NWs [10]. Over last years, some research groups succeeded [10,11] although their studies focused on absolute resistivity without further fundamental transport properties such as MR. Recently, Shim et al. [12] carried out magnetotransport properties of an individual single-crystalline (its axis oriented along the trigonal direction [001]) 400-nm-diameter Bi NW. In that case, however, the dimension of the NW was too large and the contribution of the classical MR was too high (several thousands at low temperatures) to allow the WAL effects to be observed.

In this letter, we present the magnetotransport properties of individual single crystalline Bi NWs of 100 nm-width (smaller than the mean free path) with its axis oriented along [012] using four-probe measurements in the range 5-300 K with magnetic fields up to 90 kOe. Temperature and field dependence of perpendicular MR is analyzed considering both a classical multiband model producing a residual classical MR and a weak antilocalization model accounting for one-dimensional interference below 10 K.

Bismuth NWs with an average diameter of 100 nm and 4 μm in length were fabricated by electrodeposition as described elsewhere [13]. Figure 1(a) shows the Transmission Electron Microscopy image of an individual NW revealing that they are cylindrical in shape. X-ray Diffraction and *High Resolution Transmission Electron Microscopy (HRTEM)* revealed a rhombohedral structure, the same as that of bulk Bi. The electron diffraction pattern obtained in the direction perpendicular to the long axis of the NW was indexed to the hexagonal lattice of Bi (Fig.1 (b)). Fig.1(c) shows the *Select Area Electron Diffraction (SAED)* patterns identifying the family of planes (012), (110) and (122). An exhaustive study carried out in different zones of the NW by HRTEM and SAED confirms the single crystallinity and orientation of the Bi NWs which grow along the direction [012]. No extensive defects such as grain boundaries have been observed over the length of the wire, which confirms the monocrystalline structure. The NWs have also been confirmed to be pure Bi by Energy Dispersive X-ray Spectroscopy microanalysis. A very thin amorphous oxide shell (5 nm) has been observed.

For electrical measurements on a single NW, a drop of NW-containing solution is deposited onto a thermally oxidized silicon wafer (~ 200 nm of SiO_2 on top of the Si substrate) where Aluminium *(Al)* microelectrodes have been patterned by means of conventional optical lithography. The final mask consists of large Al pads (400 μm x 400 μm), ending in four 4 μm-wide electrodes. A relatively long NW was located by means of SEM and nanoelectrodes were patterned on the NW connecting it to the Al-microelectrodes by a Tungsten (W)-based nanodeposit grown by *focused-ion-beam-induced-deposition (FIBID)* under high vacuum conditions (10^{-6} mbar). W nanodeposits are grown with a FIB energy of 30 kV and a beam current of 10 pA. This kind of deposit favours low electrical resistance as required in some applications [14]. SEM images of a 100 nm Bi-NW prepared using this technique are shown in Figure 2(a) and 2(b). The resistivity ρ measured *in-situ* [15] was found to be 6 x 10^{-4} Ω cm, which is five times higher than the ρ of bulk Bi, 1.2 x 10^{-4} Ω cm. Such an increase can be explained by an ordinary size effect [16]. Due to the cross-section of the NW of the order of the mean free path of the carrier, there is an increase of surface scattering leading to a rise of resistivity relative to bulk Bi. No modification of the resistance was observed when the NW comes into contact with ambient atmosphere, which indicates the absence of oxidation or degradation effects after exposure to ambient conditions. Magnetotransport properties have been carried out in a commercial *Physical Properties Measurement System (PPMS)* from

Quantum Design in the temperature range from 300 K down to 5 K with a low-frequency current of 100 nA. The magnetic field is applied perpendicular to the substrate plane. Measurements of the NW resistance by 4 probes are found to be ohmic at 5 and 300 K, corresponding to ρ of 1.83 x 10^{-3} Ω cm and 6 x 10^{-4} Ω cm, respectively. This fact indicates that the achieved contacts allow reliable transport measurements in the studied temperature range, and thus, the observed 5 nm-thick Bi oxide shell has been either partly removed during the contact fabrication using the ion-beam or, if still present, is not thick enough to disrupt the electrical transport.

We have studied the magnetoresistance MR (H, T) (%) = 100 x {[R(H,T)-R(0,T)]/R(0,T)} down to low temperatures in order to highlight the contribution from WAL. Figure 3 shows the magnetic field dependence of the MR. The values of MR at 90 kOe (~ 16 % at 300 K and ~ 10 % at 5 K) are significantly lower than those reported by Shim et al. [12]. We became aware that two temperature regimes can be distinguished: *i)* The high temperature regime (T > 10 K), where the field dependence of MR is essentially quadratic (Lorentz) and shows no sign of saturation at high field and *ii)* The low temperature regime (T≤ 10 K), where MR shows a dip-like shape near H = 0, which is significantly enhanced as T decreases down to 5 K. This behaviour is a signature of WAL [4]. In this low-temperature regime, the classical MR tends to dominate the magnetotransport for H > 12 kOe. It is worth noting the relative high value of H up to which WAL signatures are visible. Inset of Figure 3 (a) shows that at 90 kOe the MR increases with decreasing temperature reaching its peak value at T ~ 200 K. At low fields (H = 10 kOe) however, MR increases sharply for T≤ 10 K which, again, is a signature of localization effects [6].

We have used a standard multiband model [17] to fit the experimental MR data at T> 10 K. Each band has two parameters, resistivity ρ_i and Hall coefficient $R_i = 1/q_i n_i$, where $q_i = \pm e$ is the charge of the carrier. A two-band model, with a bulk electron and a bulk hole band, accounts for the field dependence of the MR in the temperature range 100 K < T < 300 K. For 10 K < T < 100 K, a third electron band is required. Such a minority electron band accounts for the surface states in Bi, which are highly metallic in contrast to the semimetallic nature of bulk Bi [18]. Both theoretical and experimental works [18, 19] have shown the important role of these states in the transport properties of Bi systems when dimensions downsizes to nanometer scale as occurs in Bi NWs [20]. It should be noted that the contribution of the surface states to the MR indicates that such states have not been quenched by the possible Bi oxide shell present in the NWs. The solid lines in Fig 3(a) are calculated from our two- and three-band analysis. We find that bulk electron density is larger than the bulk hole density in the temperature range 5 K < T < 300 K with a carrier density ratio n / p = 12. The surface carriers become important below 50 K, although bulk electrons are dominant. The ratio of bulk electrons to surface carrier density is 10 for these 100 nm-width NWs at low temperatures.

For T≤ 10 K the three-band model only reproduces the experimental MR curves for H ≥ 12 kOe, i. e., when classical MR dominates the magnetotransport. This is shown in Figure 3 (b) for T = 5 K. The dip in the MR for H < 12 kOe requires being analyzed in accordance with WAL theory. The correction to the resistance due to WAL in one-dimensional (1D) systems in the strong spin-orbit limit is predicted to take the form [21, 22]:

$$\frac{\Delta R_{WAL}}{R_0} = \frac{1}{\sqrt{2}} \frac{e^2}{\pi\hbar} \frac{R_{\square} L_N}{W} A_i(x) \left\{ \frac{d}{dx}\left[A_i(x)\right] \right\}^{-1} \qquad (1)$$

where $A_i(x)$ denotes the Airy function, $R_{\square}$ is the resistance per square which in the present case takes the form $R_{\square} = \rho/W$ and $x = 2\left(L_N / L_{\varphi 0} \right)^2$. $L_N = \left(D\tau_N \right)^{0.5}$ is the phase-breaking length due to quasi-elastic Nyquist scattering, which is the main contribution to the phase breaking time in low-dimensional disordered systems [22]. τ_N is the Nyquist dephasing time. $L_{\varphi_0} = \left(D\tau_{\varphi_0} \right)^{0.5}$, where $1/\tau_{\varphi_0}(B) = 1/\tau_{\varphi_0}(H=0) + 1/\tau_H$, and $1/\tau_{\varphi_0}(H=0)$ is the inelastic electron-electron scattering rate. $1/\tau_H$ is the effective dephasing rate introduced by the magnetic field (*H*), and is given by

$1/\tau_H = DW^2/12l_H^4$, and $l_H = \left(3\hbar^2/e^2AH^2\right)^{0.5}$ is the magnetic length with A the wire cross-section. In order to perform a more reliable fit to Eq (1), we have subtracted the contributions to the magnetoresistance by the classical mechanism described by the three-band model ($\Delta R_{classical}$). We have carried out a three-parameter fit (W, L_N and L_{φ_0}) to Eq (1). The experimental and calculated resistance are in very good agreement for H < 12 kOe as observed in Fig.3 (b). The values of the parameters inferred from the fit are W ~ 40 nm, L_N = 52 nm and L_{φ_0} = 63 nm at 10 K and W ~ 40 nm, L_N = 53 nm and L_{φ_0} = 65 nm at 5 K. We note that the value of the effective width obtained from the fit W is smaller than the physical width (100 nm). This difference could possibly be due to a reduction of the wire diameter caused by defect scattering by FIB irradiation, boundary scattering on some crystallographic defect or limitations in the description provided by the used model. Another feature to note is that the values of L_N are comparable to, or slightly higher than, the estimated effective width of the wire, which suggests that the transport should be intermediate between the quasi-2D and quasi-1D regimes. Attempts to fit the MR using the theoretical forms for WAL in two (2D) and three dimensions (3D) have also been made. The 3D form gives a poor fit to the data, while the 2D form gives reasonable fit only with the effective width W >> physical width of the NW. Thus, 1D fits give the best agreement with the experiment and the NW could be considered as one dimensional system with respect to WAL [7].

The relative intensity of the two effects (classical and WAL) could be altered by the wire dimensions and then WAL contribution can be tuned by reducing the wire diameter. An alternative way of enhancing the WAL contribution is the study of ultrathin Bi films with lateral size smaller than L_φ where the classical MR signal is expected to be reduced. Thus, WAL phenomena could be traced out to higher temperatures and higher magnetic fields, improving the resolution in the determination of the physical parameters derived from the analysis of the MR curves.

In summary, we have investigated the magnetotransport properties of an individual single-crystalline Bi NW 100 nm-diameter grown by electrodeposition. We achieved low-resistance ohmic contacts to single Bi-NWs that were stable from 5 to 300 K by using FIB techniques. We have analyzed the competition of classical and WAL effects as a function of temperature and magnetic field. The MR showed evidence for WAL in 1D at temperatures below 10 K, with a phase breaking length of ~ 100 nm.

Acknowledgments

This work was supported by Spanish Ministry of Science (through projects MAT2007-65965-C02-02 and MAT2008-06567-C02) and the Aragon Regional Government. N. Marcano and S. Sangiao acknowledge financial support from Spanish CSIC (JAE-doc program) and Spanish MEC (FPU program).

References

[1] A. Boukai, K. Xu and J. R. Heath, *Adv. Mater.***18**, 864 (2006).

[2] J. Heremans, M. C. Thrush, Y. Lin, S. Cronin, Z. Zhang, M. S. Dresselhaus, J. F. Mansfield, *Phys. Rev. B.* **61**, 2921 (2000).

[3] Y. Lin, S. B. Cronin, J. Y. Ying, M. S. Dresselhaus and J. Heremans, *Appl. Phys. Lett.* **76**, 3944 (2000).

[4] See for example: J. J. Lin and J. P. Bird, *J. Phys.: Condens. Matter* **14**, R501 (2002).

[5] D. E. Beutler and N. Giordano, Phys. Rev. B. **38**, 8 (1988).

[6] Z. Zhang, X. Sun, M. X. Dresselhaus, J. Y. Ying, J. Heremans, *Phys. Rev. B.* **61**, 4850 (2000).

[7] J. Heremans, C. M. Thrush, Z. Zhang, X. Sun, M.S. Dresselhaus, J. Y. Ying and D. T. Morelli, *Phys. Rev. B* **58**, 10091 (1998).

[8] K. Liu, C. L. Chien, P. C. Searson and K. Y. Zhang, *Appl. Phys. Lett.* **73**, 1436 (1998).

[9] O. Rabin, K. Nielsch and M. S. Dresselhaus, *Appl. Phys. A* **82**, 471 (2006).

[10] S.B. Cronin, Y. Lin, O. Rabin, M. Black, J. Ying, M. Dresselhaus, P. Gai, J. Minet and J. Issi, *Nanotechnology* **13**, 653 (2002).

[11] D. S. Choi, A. A. Balandin, M. S. Leung, G. W. Stupian, N. Presser, W. Chung, J. R. Heath, A. Khitun and K. L. Lang, *Appl. Phys. Lett.* **89**, 141503 (2006).

[12] W. Shim, J. Ham, K. Lee, W. Y. Jeung, M. Johnson and W. Lee, *Nanoletters.* **9**, 18 (2009).

[13] M. Plaza, M. Abuín, J. de la Venta, N. Marcano, S. Sangiao, L. Morellón, J. M. De Teresa, M. C. Sánchez, M. García and L. Pérez, unpublished.

[14] I. Guillamon, H. Suderow, S. Vieira, A. Fernandez-Pacheco, J. Sesé, R. Cordoba, J. M. De Teresa and M. R. Ibarra, *New Journal of Physics* **10**, 093005 (2008).

[15] See for example A. Fernández-Pacheco, J. M. De Teresa, R. Córdoba and M. R. Ibarra, *Phys. Rev. B* **79**, 174204 (2009).

[16] M. Barati and E. Sadeghi, *Nanotechnology* **12**, 277 (2001).

[17] N. W. Ashcroft and N. D. Mermin, *Solid State Physics* (Holt, Rinehart and Winston, New York, 1976), Chap. 12, p. 240.

[18] T. Hirahara, I. Matsuda, S. Yamazaki, N. Miyata, S. Hasegawa and T. Nagao, *Appl. Phys. Lett.* **91**, 202106 (2007).

[19] T. E. Huber, A. Nikolaeva, L. Konopo and M. J. Graf, *Phys. Rev. B.* **79**, 201304 (2009).

[20] A. Nikolaeva, D. Gitsu, L. Konopko, M. J. Graf and T. E. Huber, *Phys. Rev. B.* **77**, 075332 (2008).

[21] P. M. Echternach, M. E. Gershenson, H. M. Bozler, A. L. Bogdanov and B. Nilsson, *Phys. Rev. B*. **48,** 11516 (1993).

[22] B. L. Altshuler, A. G. Aronov and D. E. Khmelnitskii, *J. Phys. C* **15,** 7367 (1982) .

Figure captions:

Fig. 1 (Color online): (a) TEM image of 100 nm Bi NW after removing the supporting polycarbonate membrane. (b) The electron diffraction pattern taken from one of the grains. Along the NW, the diffraction patterns of different zones of NW indicate same orientation. (c) SAED pattern with the family of planes (012), (110) and (122).

Fig. 2 (Color online): (a) SEM image of the experimental configuration for the four-probe electrical measurements. The four microprobes are contacted to Al micrometric pads patterned by optical lithography in order to perform the *in-situ* measurements. The red rectangle shows the zone where the selected Bi NW is located. (b) SEM image at a higher magnification of the region where the NW is contacted with the Al micropads via the four FIBID W-nanodeposits.

Fig. 3 (Color online): (a) MR(%) as a function of field at selected temperatures in the 50 to 300 K range for the sake of clarity. Solid lines represent fits to multiband model. Inset displays the temperature dependence of the MR (%) at 10 kOe, and 90 kOe. The solid lines are guides to the eye. (b) MR as a function of field at 5 K. The solid lines in black and red represent the classical contribution and the classical + WAL correction to the resistance according to Eq. (1), respectively.

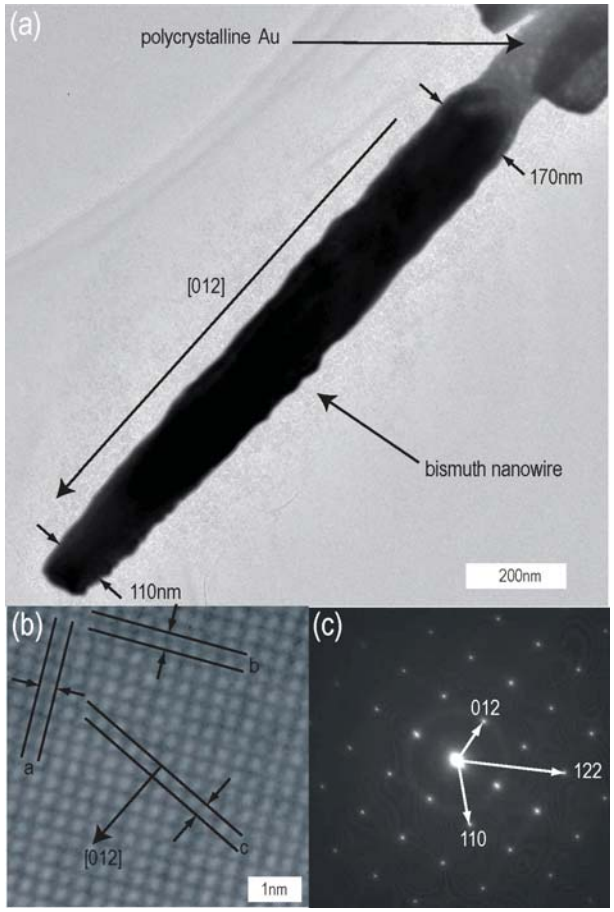
(a)
polycrystalline Au
170nm
[012]
bismuth nanowire
110nm
200nm
(b)
a
b
c
[012]
1nm
(c)
012
122
110

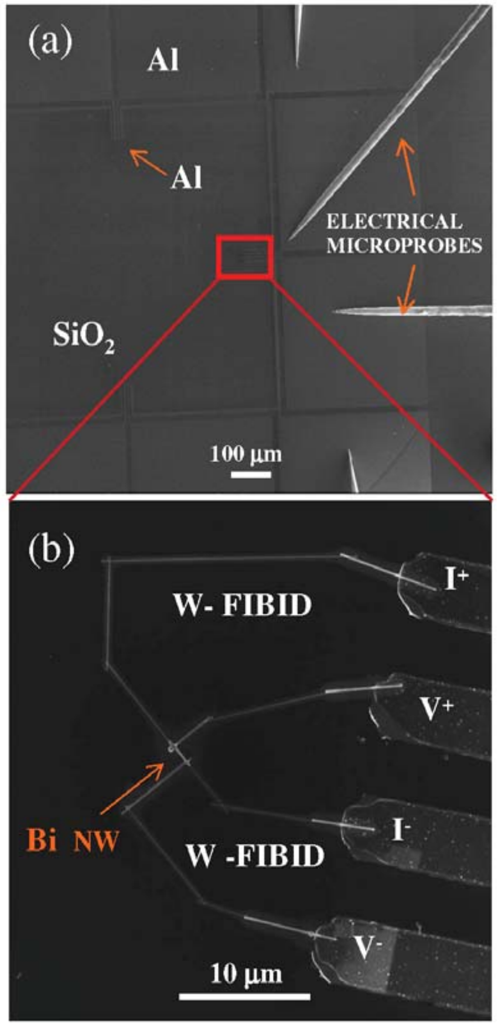
(a)
Al
Al
ELECTRICAL
MICROPROBES
SiO2
100 μm
(b)
W- FIBID
I+
V+
Bi NW
I-
W -FIBID
V-
10 μm

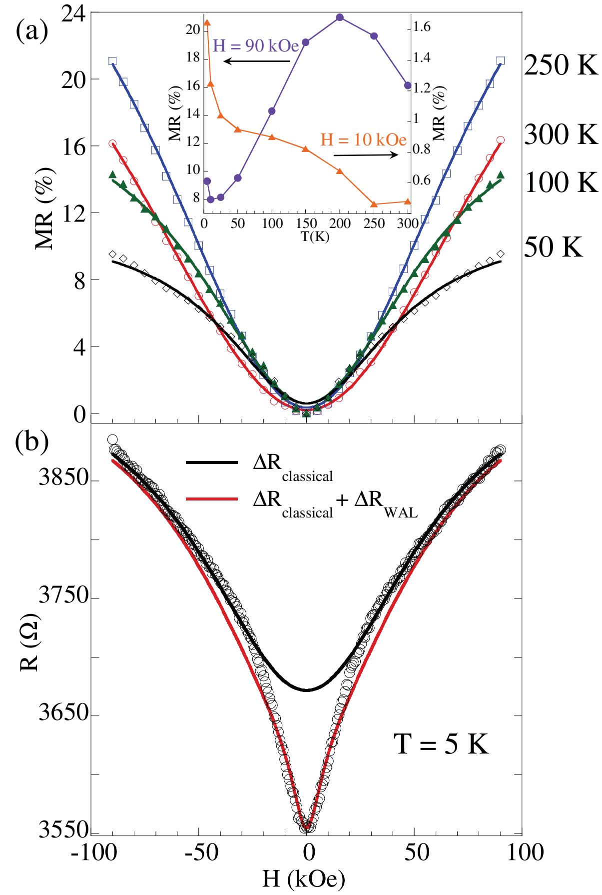
(a)
(b)
MR (%)
R (Ω)
H (kOe)
250 K
300 K
100 K
50 K
H = 90 kOe
H = 10 kOe
T(K)
ΔR classical
ΔR classical + ΔR WAL
T = 5 K